# Heat Transfer Characteristics of Thermoelectric Generator System for Waste Heat Recovery from a Billet Casting Process: Experimental and Numerical Analysis

Saurabh Yadav [1] , Jie Liu [1] , Man Sik Kong [2], Young Gyoon Yoon [3] and Sung Chul Kim [1,]*

[1]   School of Mechanical Engineering, Yeungnam University, 280 Daehak-ro, Gyeongsan-si, Gyeongsangbuk-do 38541, Korea; saurabhyadav1124@gmail.com (S.Y.); lauj@ynu.ac.kr (J.L.)
[2]   Institute of Advanced Engineering, 175-28, Goan-ro 51, Yongin-si, Gyeonggi-do 17180, Korea; mskong@iae.re.kr
[3]   Livingcare Development of Materials, 166, Gosan-ro, Gunpo-si, Gyonggi-do 15850, Korea; ygyoon@lcdv.co.kr
*   Correspondence: sungkim@ynu.ac.kr; Tel.: +82-53-810-2572; Fax: +82-53-810-4627

**Abstract:** In this study, experiments were performed to use the waste heat in a billet casting industry utilizing bismuth telluride thermoelectric generators (TEGs). Four d-type absorber plates made of copper were installed above the manufactured billet during the cooling process. Three sides of each absorber plate were attached to thermoelectric units. Therefore, a total of 12 units of the thermoelectric system were found to generate a power of 339 W. The power density of the TEG system was found to be 981 W/m$^2$ while running the system at the operating voltage of the battery energy storage system (58 V). A one-dimensional numerical simulation was carried out using FloMASTER$^{TM}$ v9.1 (Mentor Graphics Corporation, Siemens, Dallas, TX, USA) to verify the experimental results, and the numerical results were found to exhibit good agreement with the experimental results. Furthermore, a one-dimensional numerical simulation was carried out to obtain the heat transfer characteristics at varying flow rates of cold water (Reynolds number = 2540–16,943) and at different inlet temperatures (10–25 °C) for the cold side of the TEG. The results indicate that the performance of the thermoelectric generator increases with an increase in the cold-water flow rate and a decrease in the inlet temperature of the cold water.

**Keywords:** waste heat recovery; heat exchanger; heat source; thermoelectric generator; Radiative heat exchanger; numerical analysis; FloMASTER$^{TM}$

## 1. Introduction

The worldwide desire to reduce the use of conventional energy sources is at odds with the increased demand for energy for economic growth. Therefore, the focus has been on the simultaneous use of various renewable energy sources and an improvement in the utilization of waste heat produced in various industrial processes [1,2]. It is estimated that of the 474 PJ of global energy consumption, 52% of the heat is wasted through exhaust gas and effluents. Various industries are the primary sources of waste heat generation, accounting for approximately 22% of the total energy used annually, which results in inefficient and uneconomical industrial facilities [3]. Inefficient industrial systems also lead to increased greenhouse gas emissions, resulting in global warming. Therefore, it is expected that the recovery of waste heat from industrial processes will lead to more efficient and economical industrial facilities and a simultaneous reduction in greenhouse gas emissions [4]. Industrial processes, products, and equipment are the primary sources of waste heat, which is lost in various modes, such as conduction, convection, and radiation [5]. Waste heat recovery (WHR) systems are usually introduced based on their temperature ranges. These systems capture and transfer waste heat from an industrial process as a secondary energy source [6]. Therefore, different heat recovery systems are employed to capture and recover waste heat from industrial processes, such as air

preheaters, recuperators, regenerators, heat wheels, and run around coils, economizers, and waste heat boilers. These systems are complex and employ various thermodynamic cycles, and so, they are sometimes unsuitable for WHR systems [6].

Numerous thermoelectric generator (TEG) systems are installed for waste heat utilization in various industries, such as automobile, shipping, aircraft, and space industries. These TEG systems are very simple and do not have the complexity of moving parts [2]. TEG systems have low efficiency, but this disadvantage is offset by advantages such as energy savings and emission reduction. In turn, this has created a great interest in recovering waste heat by utilizing TEG systems in industries that have an enormous amount of waste heat [1–6]. This has resulted in various studies for recovering waste heat using TEG systems. Kaibe et al. [7] performed thermoelectric generation experiments in a carburizing furnace at Komatsu Ltd., Awazu plant. The residual carburizing gas was found to have a burning power of 20 kW, and a heat exchanger was employed to heat the hot side of a Bi-Te-based TEG system consisting of 16 modules. It was reported that 20% of the available heat was collected using the heat exchanger, and nearly 214 W of the power was generated through the TEG system. Experimental investigations and mathematical studies were conducted by Aranguren et al. [8,9] to recover waste heat from a combustion chamber using a TEG system. The investigation was conducted to evaluate the performance of the cooling system of the TEG and discuss the results for finned and heat pipe-type cold heat exchangers. A potential production of 100 W/m$^2$ was reported by utilizing the industrial chimney for waste heat on a ceramic tile furnace with a flue gas mass flow of 18,400 Nm$^3$/h. The authors also found that flue gases at a temperature of 187 °C can generate 136 MWh of power per year. Research was conducted to investigate the water heat recovery in the casting of steel at JFE Steel Corporation (JFE) in Japan [10–12]. An enormous amount of radiant heat was wasted during steel casting, and it was identified as a target source for waste heat recovery. A total of 896 thermoelectric modules made of bismuth telluride (covering a total area of 4 m × 2 m) were installed with a capacity of approximately 10 kW. The total power output was 9 kW using the TEG system. In the steel forging industry, investigation was made by Ebling et al. [13] of recovery of the waste heat from the steel cooling process utilizing a 50 bismuth telluride TEG system. The waste heat from the final product was recovered using a copper absorber plate through radiative heat transfer. The authors reported the source temperature to be 1300 °C while utilizing the TEG system, and a power of 388 W was produced with an efficiency of 2.6%. Research was also conducted by Yazawa et al. [14] to recover the waste heat through a glass melting furnace in a glass-shaping industry utilizing a TEG system. The temperature of the target heat recovery source was found to be approximately 1500 °C. The results indicated a maximum power generation of 55.6 W, while an assumption was made that the TEG module was a direct conduction type. Luo et al. [15] utilized a Bi$_2$Te$_3$–PbTe-based hybrid TEG system to recover waste heat in the Portland cement production industry. The authors reported about 10–15% of the energy dissipation into the atmosphere directly from a rotary kiln surface with a capacity of 10 MW heat loss. The authors carried out a theoretical investigation employing a mathematical model and reported a total 210 kW power production using 20 units of 3480 thermoelectric modules with an area of 30 × 30 mm$^2$. Jang et al. [16] performed three-dimensional simulations and experiments to recover waste heat from the venting flue gas in a chimney. They utilized plate-fin heat sinks on the hot side of the TEG to recover the waste heat and investigated the heat transfer performance across the system at different flue gas velocities (3, 5, and 10 m/s) and flue gas temperatures (T$_{gas}$ = 500, 600, and 700 K). The investigation was carried out for various parameters such as the plate-fin height (H$_{fin}$ = 0–100 mm) and the number of fins (*n* = 4–8). The results indicated that the power density increases with the increase in flue gas velocity, increase in the number of fins, and fin height. The maximum power density was reported for a source temperature of 700 K. Experimental and mathematical studies of the WHR in silicon casting using a bismuth telluride TEG system were carried out by Borset et al. [17]. The investigation was conducted for a casting area of 0.25 m$^2$ and obtained 160 W/m$^2$ power density, while the maximum temperature difference across the modules was found to be 100 K. A one-dimensional mathematical model was also

developed to predict the power generation in the experimental analysis and suggested that an increase in the heat transfer coefficient at the cold side of the TEG may enhance TEG power density up to 900 W/m$^2$. The heat pipes assisted TEG (HP-TEG) system was used to recover waste heat from the exhaust system of an automobile by Cao et al. [18]. The authors reported that the power output of HP-TEG increases with increase in exhaust temperature and cold water flow rate. The maximum of efficiency of the TEG system was reported to be 2.58% in their study. A lab-scale bismuth telluride-based TEG sandwiched between two heat pipes was developed to recover waste heat by Remeli et al. [19]. The investigation was made to evaluate heat transfer rate, effectiveness of heat pipe heat exchanger, and maximum output power of the TEG system. The highest heat exchanger effectiveness was reported to be 41% at a cooling air speed of 1.1 m/s. The TEG system was found to produce 7 W of electric power with a conversion efficiency of 0.7%.

It can be noticed from the above literature that studies have been carried out to recover waste heat in various industrial processes. Most of these studies have utilized a flat surface for the absorber plate, and a few studies have reported the use of heat pipes to extract heat from the targeted source of waste heat. In addition, limited studies have been conducted to investigate the cooling performance of a TEG system at varying flow rates and inlet fluid temperatures. Moreover, experimental studies were conducted using TEG systems with different numbers of modules to improve power density. Considering these limitations, we have presented a study [20] that identifies a suitable geometry of the absorber plate through three-dimensional numerical simulation for recovering the maximum waste heat in the cooling process of billet casting. It has been found in our previous numerical study that the d-type absorber plate provides a higher heat transfer performance compared to the *n*-type and o-type absorber plates. Furthermore, in the previous work, experiments have been performed for a TEG system using an *n*-type absorber plate only to compare our numerical results for the heat transfer characteristics of the absorber plate. Moreover, 740 W/m$^2$ of power density has been achieved by employing the maximum power point tracking (MPPT) model through experimental investigation utilizing an *n*-type absorber plate [20]. However, in the previous work, the experiment has not been performed using a d-type absorber plate, and numerical investigation has not been carried out to obtain the TEG characteristics. In addition, numerical and experimental investigations have not been carried out to obtain the TEG characteristics utilizing a d-type absorber plate. In addition, experimental and numerical investigations have not been carried out to obtain the heat transfer characteristics of TEG system for the various flow rates and different inlet temperatures of cooling water at the cold side of TEGs.

To overcome the above-mentioned limitations and following our previous work [20], an attempt has been made to improve the power density up to 1 kW/m$^2$ using a d-type absorber plate and a modified TEG system in the present study through the experimental investigation. Experimental results for heat transfer characteristics and TEG characteristics are also verified utilizing one-dimensional numerical simulation through commercially available software FloMASTER$^{\text{TM}}$ v 9.1. In addition to this, numerical study also reports the evaluation of heat transfer characteristics of the TEG system for various cooling flow rates (0.03–2.0 kg/s) of water at different inlet temperatures (10–25 °C). Results are also evaluated for the maximum power output and the corresponding TEG efficiency utilizing an MPPT model for the thermal characteristics of TEG obtained by one-dimensional numerical simulation for varying cooling flow rates at different inlet temperatures of water.

## 2. Experimental Test Facility and Procedure

In the brass billet casting industry at Gwangmyeong-Si, the Republic of Korea, two continuous lines of billets after the casting process were first cooled through an air injector and later cooled with a water injector. An enormous amount of heat is liberated with two continuous billet lines, and loose heat to the ambient is considered a targeted zone for the recovery of waste heat. The exposed length in the ambient environment is found to be 3600 mm between the air and water injector, of which 1800 mm of the length of the two

continuous lines of the billet is available for the use of waste heat recovery. The center-to-center distance between these two continuous lines is found to be 500 mm, while the diameter of each billet is found to be 240 mm. Figure 1 shows a schematic view of the test facility, which includes a TEG system, direct current (DC) electronic loader, battery system, main controller, and computer system. Figure 2 shows a photographic view of the waste heat recovery system utilizing thermoelectric generators. Here, billets are surrounded by four sets of d-type absorber plates (heat exchangers) made of copper. Each absorber plate has a length of 600 mm with 0.48 m$^2$ of total heat transfer area on the TEG side. Each d-type absorber plate covers the billet from three sides, and each side of the absorber plate is attached to a thermoelectric generator and is manufactured by LIVINGCARE Co., Ltd. The TEG at the upper surface of the absorber plate was labeled 'a', while the TEGs on the left and right-hand sides of the absorber plate were labeled 'b' and 'c', respectively. Therefore, set-1a refers to the TEG at the upper surface of the absorber plate labeled set-1 as shown in Figure 2. A total of 12 generators were used for power generation from waste heat. These TEGs ($N_p$ = 12) were connected in parallel. Each TEG system is constructed with $n$ = 8 thermoelectric modules connected in series. The arrangement of the modules within each of the 12 TEG systems is shown in Figure 3. Each thermoelectric module consists $n$ = 391 pairs of both $p$-type and $n$-type semiconductors made of bismuth tellurium material. These semiconductors are connected together with copper electrodes and are sandwiched between two electrically nonconductive (electric insulator) ceramic plates made of $Al_2O_3$. The size and material used for the insulators, electrodes, and semiconductors are listed in Table 1, while Table 2 describes the material properties.
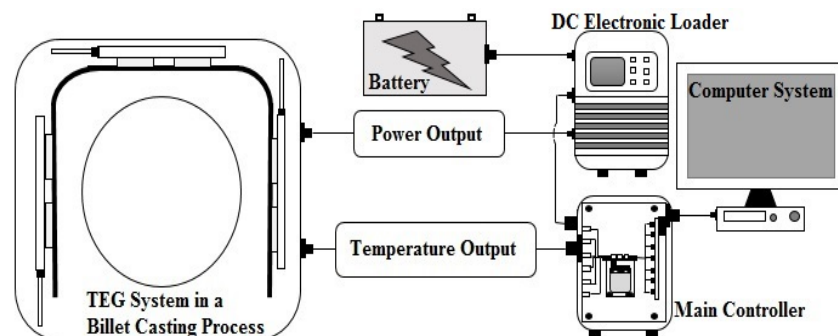


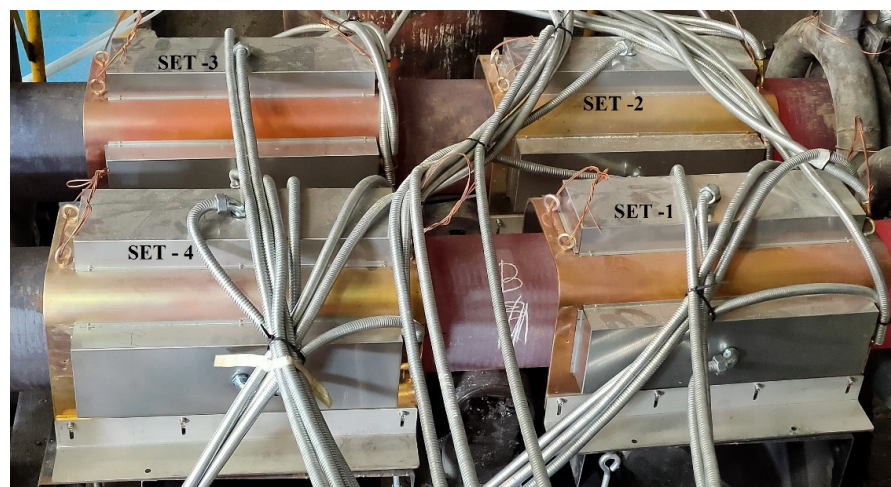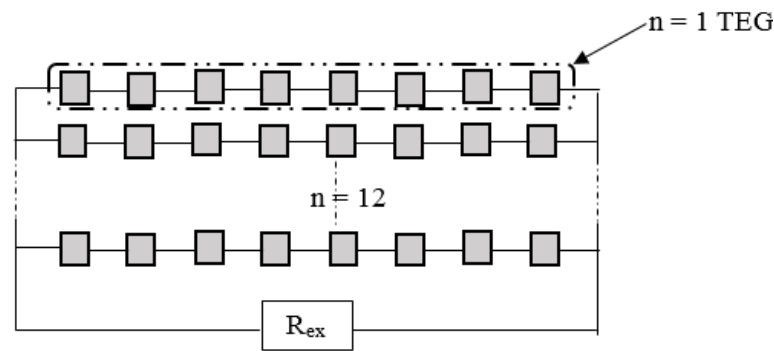**Figure 1.** Schematic view of the experimental test facility.



**Figure 2.** Photographic view of the waste heat recovery system using thermoelectric generators (TEGs).

**Figure 3.** Arrangements of thermoelectric generators.

**Table 1.** Specification of semiconductor.

| Module Specification | Material | Size (L × W × H) mm$^3$ |
|---|---|---|
| Insulator | Ceramic (Al$_2$O$_3$) | $60 \times 60 \times 1$ |
| Electrode | Copper (C1100) | $3.7 \times 1.6 \times 0.3$ |
| Semiconductor | Bi$_2$Te$_3$ | $1.5 \times 1.5 \times 0.3$ |

**Table 2.** Properties of material.

| Properties | Ceramic | Copper | $p$–Type | $n$–Type |
|---|---|---|---|---|
| Thermal conductivity (W/mK) | 25 | 387.5 | 1.3 | 1.1 |
| Electrical resistivity ($10-5$ Ωm) | - | - | 4.1 | 3.7 |
| Seebeck coefficient (μV/K) | - | - | 203.7 | −172.1 |

The hot-side TEG ceramic plate is attached to the absorber plate surface, while the cold-side ceramic plate is attached to a cooling block of the TEG. A soft graphite sheet with high thermal conductivity is used to couple the hot-side ceramic plate with the absorber plate and the cold-side ceramic plate with the TEG cooling block to ensure low thermal contact resistance. The cooling block of the TEG consists of a 0.015 m diameter serpentine pipe made of stainless steel. Cold water is allowed to flow continuously in this pipe to maintain the low temperature of the TEG on its cold side.

During the experiments, thermoelectric generators are installed for 28 h and continuously cooled with cold water on the cold side of the TEGs. The inlet water temperature (20 °C) and flow rate (0.03 kg/s) are kept constant during the experiments. The temperature measurements are taken at the billet surface, the hot and cold sides of the TEG systems, and at the water inlet/outlet, using a K-type thermocouple (Omega; accuracy: ±0.5 °C) at 10 s time intervals. During the cooling process of the billet, a thermocouple was attached to the billet surface to measure the change in its surface temperature, while the billet traveled toward the water injector from the air injector in its axial direction. Figure 4 shows a schematic view of the various temperature measurement for the TEG system during the experiments. These temperatures were recorded through the main controller comprising the data acquisition system (GRAPHTEC, model: midi LOGGER GL240). The thermoelectric generators are connected to a varying DC electronic loader (GW Instek, model: PEL-3111 range: 1.05, 1.5, 150, and 210 A) and are used to regulate the power of the installed TEG system. The power through the electronic loader is regulated by varying the external resistance (R$_{ex}$) of the TEG system. The regulated power is supplied to a battery energy storage system (make: HLB power, model: RE5.4P3.0C/2PK, capacity: 5.4 kW; operating voltage: 58 V) at its rated operating voltage to store the generated power from the TEG. Battery energy storage and varying electronic load systems are connected to the main controller to record the power output from the TEG system. Furthermore, a computer unit is used to view and record the entire output of the TEG system connected to the main

controller. The final readings are recorded after the establishment of thermal equilibrium when a constant power output is observed.
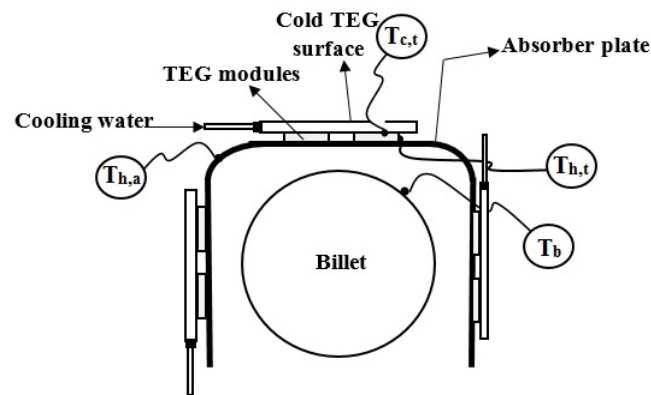


**Figure 4.** Experimental measuring locations of temperature in the TEG system.

## 3. One-Dimensional Numerical Study

In the present study, a one-dimensional numerical simulation has been implemented using commercially available software FloMASTER$^{TM}$ V 9.1 to validate the experimental results of the TEG system by obtaining the heat transfer characteristics of the TEG. FloMASTER$^{TM}$ enables a simple model to be established for complex heat transfer systems and includes the ability for a complete analysis of the heat transfer characteristics to be made quickly and effectively. FloMASTER$^{TM}$ consists of various components that can be connected in series and parallel with the help of nodes. The components used in the present study include a heat source (billet), radiation and convective arm, solid bar, and thermal bridge. The radiation and convection arms enable radiative and convective heat transfer during the process. Solid bars have been used for the absorber plates, electrodes, ceramic plates, semiconductors (*p*- and *n*-type), and cooling plates. A thermal bridge has been used in the cooling loop of the TEG system that enables direct contact with two fluid nodes and one solid node to model the heat flow from the cooling plate to the heat exchanger. It should be noted that the convective arm for the natural convection works on the Nusselt number correlation with the Rayleigh number, whereas the thermal bridge utilizes the Dittus–Boelter correlation for the turbulent flow regimes. Figure 5 shows the heat transfer network used for the one-dimensional simulation. Here, one can see heat transfer in the network that shows eight modules of one TEG system connected in parallel thermally. These modules are electrically connected in series.

Figure 6 shows the temperature distribution at various locations across the TEG layers through the source during numerical study, where $T_{h,ab}$ and $T_{h,a}$ denote the absorber plate temperature at the billet and TEG sides, respectively, at respective locations $x_0$ and $x_1$. $T_{h,t}$ and $T_{c,t}$ represent the hot-and cold-side TEG temperatures, respectively, at locations $x_2$ and $x_3$. The cooling plate temperature is denoted by $T_{c,p}$ at location $x_4$.

The present numerical analysis was performed to estimate the heat transfer characteristics of a TEG system for set-1a. The study was conducted for steady-state conditions, while segmentation analysis, component interaction, and zero heat flow heat transfer were enabled for the analysis. The numerical calculation of FloMASTER$^{TM}$ is based on the fluid network analysis method, as shown in Figure 6. The thermal energy source (billet) has a variation in the surface temperature in its axial direction; therefore, it exhibits transient behavior. However, constant temperature for the source was used to examine the TEG characteristics for the present case of one-dimensional heat transfer by considering all surfaces to be isothermal normal to the heat transfer direction. In addition, the one-dimensional study considered a uniform heat flux across the surface of the TEG system.
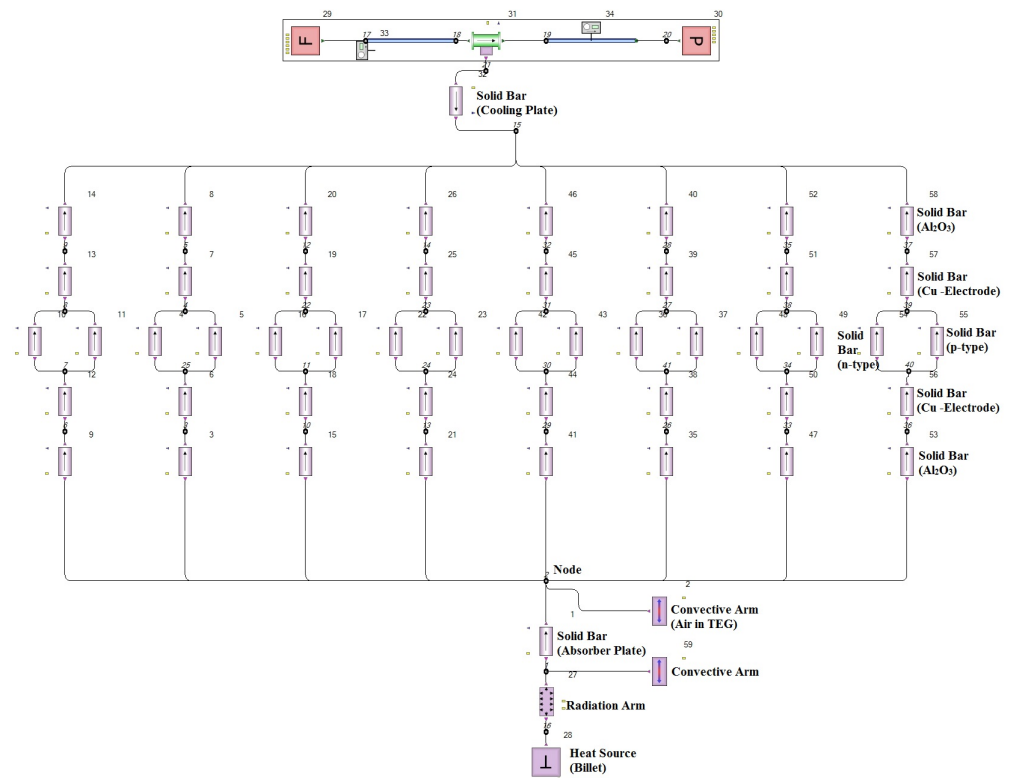
**Figure 5.** One dimensional heat transfer network used in FloMASTER$^{TM}$ for the analysis.
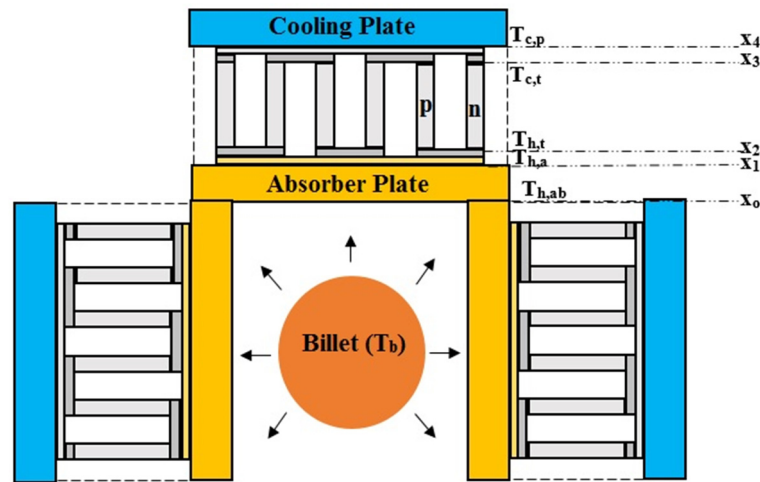


**Figure 6.** Temperature distribution at various locations across a TEG in numerical simulation.

### 3.1. Boundary Condition

A constant temperature at the inlet (average temperature of the billet at 540 °C) is used for the temperature source while the brass emissivity is maintained at 0.6 [18]. The convective arm is used for natural convection between the billet and the absorber plate. A water loop is used for the cooling process; therefore, a constant flow rate of water and temperature of 0.03 kg/s and 20 °C, respectively, are given for the outlet boundary conditions. The dimensions and properties of the TEG surfaces are listed in Tables 1 and 2, respectively. The heat flux in the TEG model is given by Equation (1).

$$Q_{in} = \varepsilon\sigma(T_b^4 - T_{h,ab}^4) + h_{ab}A(T_b - T_{h,ab}) \tag{1}$$

where $\sigma$ is the Stefan–Boltzmann constant, $\varepsilon$ is the radiative properties of the arrangement of two surfaces, $h_{ab}$ is the convective heat transfer coefficient for the absorber surface at $x_0$, and $T_b$ is the surface temperature of the billet. The heat flux out of the TEG at $x_4$ is given by Equation (2).

$$Q_{out} = U_{cp}(T_{cp} - T_{cw}) \tag{2}$$

where $h_{cp}$ is the overall heat-transfer coefficient of the cooling plate, and $T_{cp}$ and $T_{cw}$ are the temperatures of the cooling plate and cooling water, respectively.

### 3.2. Transport Equations

The transport of heat and charge through each solid component is described by the following one-dimensional flux equations:

$$q_i = -K_i \frac{dT}{dx} + \frac{S_i^* T}{F} j_i \tag{3}$$

$$j_i = -\frac{S_i^*}{F r_i} \frac{dT}{dx} - \frac{1}{r_i} \frac{d\phi}{dx} \tag{4}$$

where $i$ refers to each solid component (absorber plate, electrical insulator, electronic, and $p$- or $n$-type semiconductor), $K_i$ is the thermal conductivity, $F$ is Faraday's constant, $r_i$ is the electrical resistivity, and $S_i^*$ is the transported entropy of the charge carrier. Equation (3) states that heat can be transported by conduction and electric currents, while Equation (4) states that the electric current and potential are generated through a temperature gradient. If there is no charge transport across the TEG, Equation (3) can be reduced to Fourier's law, as shown in Equation (5).

$$q_i = -K_i \frac{dT}{dx} \tag{5}$$

After a successful numerical analysis, the final temperatures between the surfaces of various layers of the TEG are obtained. Based on these temperatures, the hot- and cold-side heat fluxes are calculated using Equations (6) and (7), respectively.

$$Q_h = \alpha_{pn} I T_{h,t} + K_{pn}(T_{h,t} - T_{c,t}) - 0.5I^2 R_{pn} \tag{6}$$

$$Q_c = \alpha I T_{c,t} + K_{pn}(T_{h,t} - T_{c,t}) + 0.5I^2 R_{pn} \tag{7}$$

where $T_{h,t}$ and $T_{c,t}$ are the hot- and cold-side temperatures of the TEG, respectively, while $K_{pn}$, $\alpha_{pn}$, and $R_{pn}$ are the thermal conductivity, Seebeck coefficient for one pair of semiconductors, and electric resistance across the semiconductors, respectively. $I$ represents the current flow across the TEG system and is measured experimentally.

Here, the power ($P$) generated across the TEG system and the efficiency ($\eta$) of the TEG system can be evaluated using Equations (8) and (9), respectively.

$$P = Q_h - Q_c \tag{8}$$

$$\eta = \frac{P}{Q_h} \tag{9}$$

### 4. Results and Discussion

In the billet casting industry, tests were performed to measure the recovery of waste heat from the billet cooling process. Four sets of d-type absorber plates, each with three TEG systems, were used for power generation. The final readings were recorded after the establishment of thermal equilibrium when a constant power output was observed. A steady-state one-dimensional heat transfer numerical analysis was performed using the FloMASTER$^{TM}$ software for one TEG system (set-1a) consisting of eight modules. During the experiments, the temperature at the hot side ($T_{h,t}$) and cold side ($T_{c,t}$) of the TEG system and absorber plate temperature were measured by providing four thermocouples on each

surface and are located equidistantly along the length of the TEG system. The temperatures are measured with the use of K-type thermocouples with an accuracy of ±0.5 °C. The relative standard deviation of the hot- and cold-side TEG temperatures are found to be 3.04% and 3.12% respectively, and therefore, one can consider the average value of hot- and cold-side temperatures of TEG system. The relative standard deviation in the absorber plate surface temperature is found to be 4.1%, which signifies less temperature variation in the absorber plate temperature along the length of the billet. This may be due to the fact that the axial heat transfer takes place within the absorber plate along the length of billet. This further leads to less temperature variation in an array of the TEG system, and therefore, the average value of the temperatures are considered for the analysis. It was observed that the temperature of the billet surface along the length of the billet varied owing to the billet cooling process. Figure 7 shows the variation in the billet temperature along the axis for the length of one d-type absorber plate (set-1a). The average temperature of the billet was found to be 540 °C; therefore, a constant source temperature of 540 °C has been assumed for the one-dimensional numerical analysis. Natural convection and radiation heat transfer were considered in the numerical heat transfer analysis.
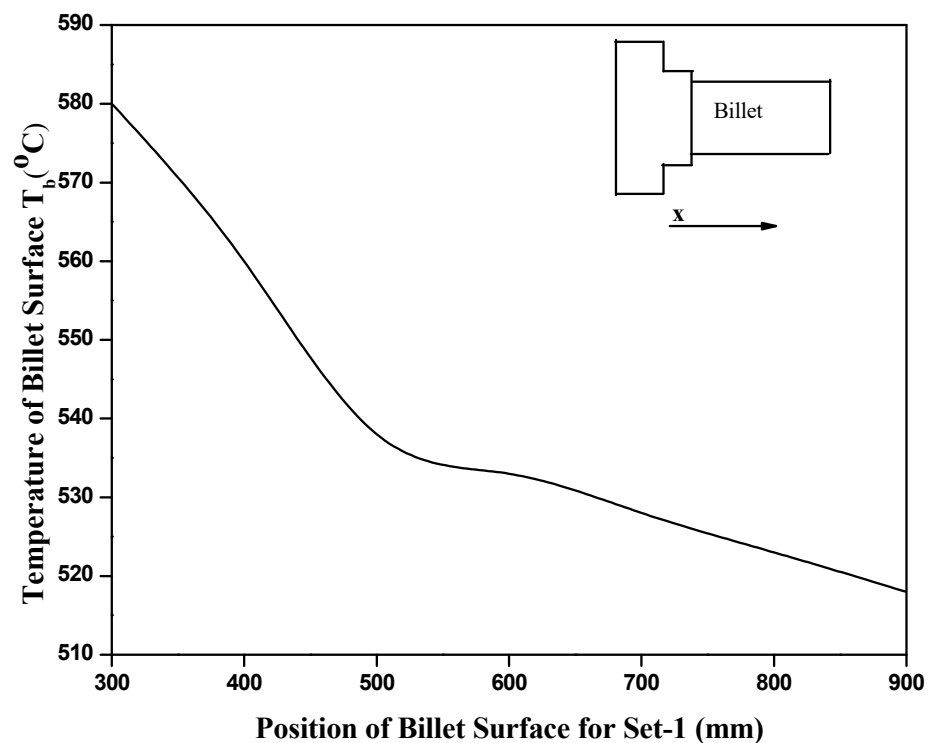


**Figure 7.** Variation in surface temperature of billet for the length of one absorber plate.

Table 3 shows the average experimental value of temperatures obtained for twelve sets of TEG systems. The average billet temperature for the different sets of absorber plates is found to decrease along the length of billet, resulting in a corresponding decrease in the absorber plate temperature. This leads to a decrease in the average temperature of the hot and cold side of various sets of TEG systems along the length of the billet. All TEG systems are connected in parallel electrically with an electrical loader. The electrical loader allows all the sets of the TEG system to be operated at the operating voltage of the battery, and the total produced power is obtained from the experiments for the TEG system. Therefore, an attempt has been made to evaluate the theoretical power of one module for each TEG set based on experimentally measured temperatures of an individual set of a TEG system utilizing Equations (6)–(8) and Tables 1 and 2. Furthermore, the theoretical power of one module of each set is compared with set-1a. The maximum deviation in the theoretical power output is found to be −3.368% for set-4c. It is worth noticing that the deviation in

the temperature difference of the hot- and cold-side TEG systems is small compared to the temperature difference of the other set, and the maximum deviation is found to be 2.0 °C for set-2a and set-4c in the temperature difference of the hot- and cold-side TEG system. This may be due to the fact that all TEG sets are identical and have the same characteristics, which further leads to less deviation in the theoretical power output of one module for each set. In addition, the average value of theoretical power output of one module is found to be 3.504 W, while the experimental average value of the power output for one module is found to be 3.53. Therefore, the average experimental power output of one module of set–1a is considered for further analysis.

**Table 3.** Temperatures of various sets of TEG systems and corresponding theoretical power of one module.

| TEG Set No. | $(T_b)_{avg}$ in (°C) | $(T_{h,t})_{TEG}$ in (°C) | $(T_{c,t})_{TEG}$ in (°C) | $(\Delta T)_{TEG}$ in (°C) | Theoretical Power of one Module for Battery Rated Voltage (W) | Percentage Variation of Power with Set-1a (%) |
|---|---|---|---|---|---|---|
| 1a |  | 207.5 | 122.2 | 85.3 | 3.533 | 0 |
| 1b | 540.0 | 206.1 | 121.0 | 85.1 | 3.518 | −0.424 |
| 1c |  | 206.6 | 121.6 | 85.0 | 3.511 | −0.623 |
| 2a |  | 212.8 | 126.7 | 86.1 | 3.611 | 2.207 |
| 2b | 543.2 | 210.5 | 124.6 | 85.9 | 3.590 | 1.613 |
| 2c |  | 209.1 | 123.3 | 85.8 | 3.583 | 1.415 |
| 3a |  | 194.6 | 109.8 | 84.8 | 3.483 | −1.415 |
| 3b | 512.6 | 193.4 | 108.9 | 84.5 | 3.454 | −2.236 |
| 3c |  | 193.9 | 108.3 | 84.6 | 3.462 | −2.009 |
| 4a |  | 192.4 | 107.9 | 84.5 | 3.454 | −2.236 |
| 4b | 509.3 | 192.1 | 107.8 | 84.3 | 3.432 | −2.859 |
| 4c |  | 191.4 | 107.3 | 84.1 | 3.414 | −3.368 |

Figures 8 and 9 depict the thermoelectric generator polarization curve and power curve obtained by activating the electronic load ($R_{ex}$) after the establishment of thermal equilibrium across the generators for one module of set-1a. The polarization and power curves were calculated based on the experimental and numerical data. The numerical results show a linear relation in the polarization curve, whereas the experimental results are not perfectly linear. This may be due to the fact that the experiments were conducted in real-time conditions in an industrial setting. Small changes in atmospheric conditions during the experiments may cause variations in radiant and convective heat transfer to the absorber plate surface from the billet surface, which also leads to fluctuations in the temperature difference across the TEG. This may be the reason for the variations in the experimental results. The maximum variation in the voltage obtained for the experimental analysis was found to be 4.4% of the numerical results. Figure 9 shows the variation in the power with current for one module of set-1a. The maximum power for one module was found to be 3.81 W for a current flow of 0.6 A across one module. $R_{ex}$ has been used to set a maximum current of 0.49 A in order to maintain the operating voltage (58 V) of the battery system. Therefore, the maximum generated power across one module of set-1a was 3.53 W, leading to a maximum of 339 W power output with the use of four sets of d-type absorber plates consisting of 12 TEG systems.
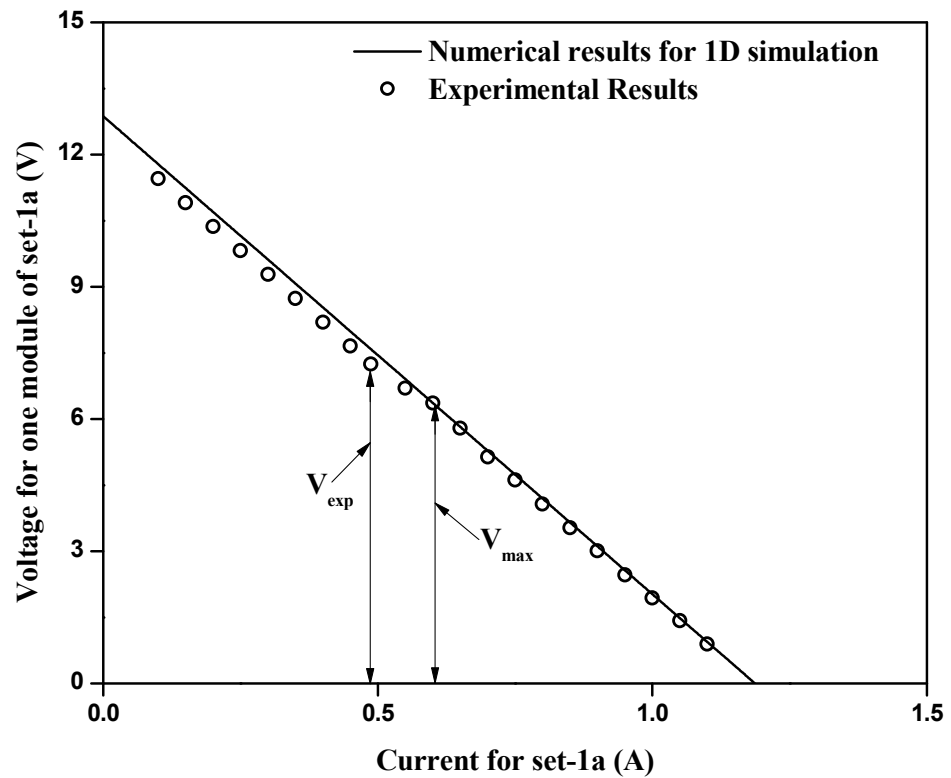
**Figure 8.** Thermoelectric generator potential as a function of total current.
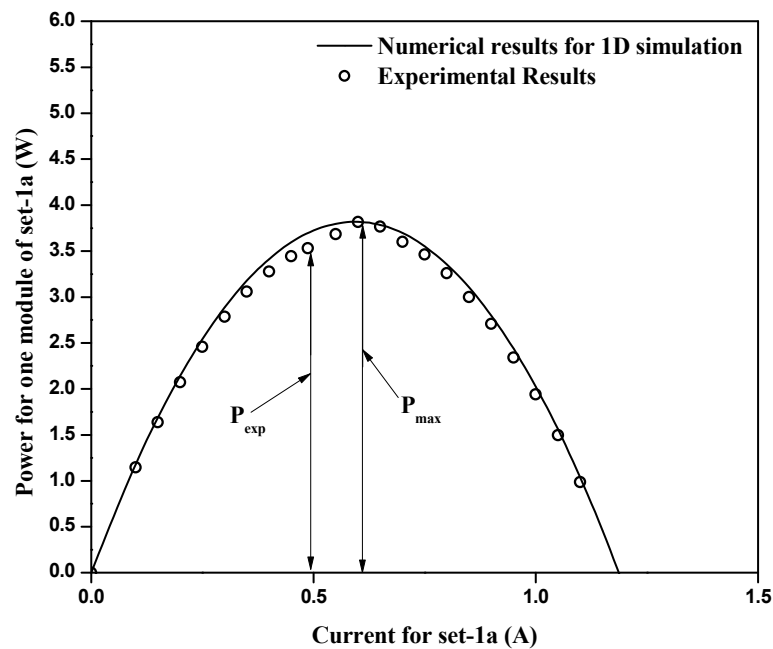


**Figure 9.** Thermoelectric generator power as a function of total current.

An attempt was made to obtain the temperature variation across a TEG system in the longitudinal direction of the billet through numerical analysis (Figure 10). The largest temperature drop of 321.92 °C was observed between the billet surface temperature and billet-side absorber plate temperature. The radiation and free convection heat transfer took place between the billet and absorber plate. This may be the reason for the large temperature drop. In addition, heat transfer across the absorber plate and TEG layers took place through conduction, and the large temperature drop observed between the

hot and cold layers of the TEG was 87.6 °C. This may be due to the fact that the thermal conductivities of semiconductors and air are less than 1% that of the thermal conductivity of the absorber plate (Table 2). This is expected to be the largest drop in temperature between the hot and cold layers of the TEG and is beneficial for higher power generation during waste heat recovery.
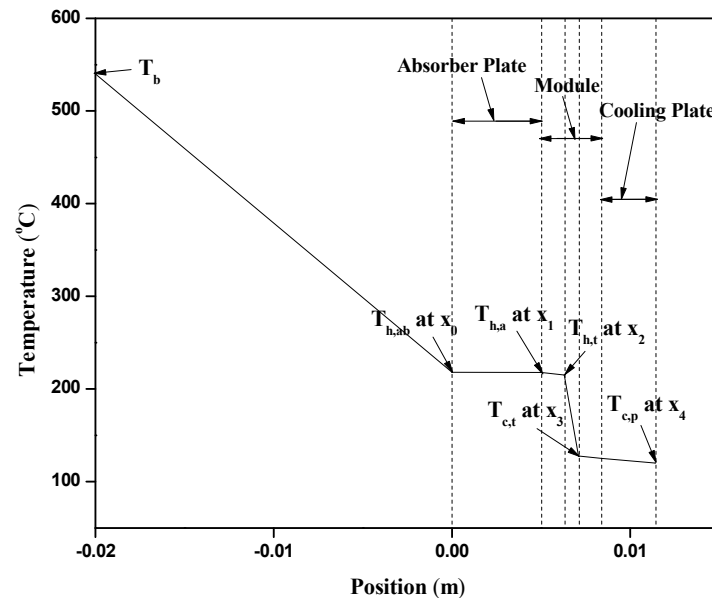


**Figure 10.** Temperature variation across a TEG system in the longitudinal direction of a billet obtained by numerical study.

Table 4 presents a comparison between the experimental and numerical results for set-1a of the thermoelectric-based waste heat recovery system. It can be seen that the experimental average temperatures of the hot and cold sides of the TEG are lower than the results obtained from the one-dimensional numerical simulation. It should be noted that during the experiments, the surface temperature of the billet varied along its length. In addition, the absorber plate average temperature was found to be affected during the experiments due to variations in atmospheric conditions (real-time experimental conditions), resulting in variations in radiant and convective heat transfer between the billet and absorber plate. This further led to variations in the hot- and cold-side average temperature of the TEG surface. In the one-dimensional numerical simulation, a constant temperature of the source (billet surface) was used for the analysis, resulting in a uniform surface temperature at the hot and cold sides of the TEG. Furthermore, the cold-side contact area for the cooling loop is the same as that of the cold plate area, leading to a higher heat transfer at the cold side of the TEG. These may be the reasons for the variation between the experimental and numerical results of the cold and hot sides of the TEG temperatures. A similar reason can be given for the variation in power generation of one TEG module and the efficiency of the TEG system obtained during experimental and numerical studies for set-1a. The maximum power generated from one TEG module of set-1a was found to be 3.53 and 3.7 W for the experimental and numerical studies, respectively, at the operating voltage of the energy storage battery. The efficiency of the TEG system was found to be 1.48% and 1.5% for the experimental and numerical studies, respectively. A maximum power of 3.82 W can be generated for one module of set-1a using the maximum power point tracking (MPPT) model for the TEG system (Figure 9). This leads to a maximum power generation of 367 W using the same setup of four d-type absorber plates consisting of twelve thermoelectric generators. The maximum power density is found to be 981 W/m$^2$ with the use of an operating voltage-based battery storage system, and the maximum achievable power density was found to be 1061 W using the MPPT model of power generation.

**Table 4.** Comparison of experimental and numerical results.

| Parameter | Experimental Result | Numerical Result | Variation (%) |
|---|---|---|---|
| Hot-side TEG temperature (°C) | 207.5 | 215.3 | 3.62 |
| Cold-side TEG temperature (°C) | 122.2 | 127.7 | 4.31 |
| Power produced by one module of set-1a (W) | 3.53 | 3.7 | 4.59 |
| Efficiency of one TEG module for set-1a (%) | 1.48 | 1.5 | 1.34 |

The present experimental investigation is limited to one cooling flow rate and temperature of water owing to industrial constraints. Therefore, an attempt has also been made to study the effect on the TEG performance and heat transfer characteristics of a cold-side TEG system with a varying inlet temperature of cooling water (10–25 °C) and variable flow rate (0.03–0.2 kg/s) for set-1a using a one-dimensional numerical simulation in FloMASTER™. Figure 11 depicts the variation in the inlet and outlet water temperature differences at various inlet temperatures of water and cooling fluid flow rates. The Reynolds number (Re) for water varies between 2540 and 16,943. It is observed that the temperature difference between the inlet and outlet temperatures of water is almost independent of the inlet temperature. However, the temperature difference decreases with an increase in the cooling flow rate. This may be due to the fact that the rise in the cooling flow rate increases the mass heat-carrying capacity of water.
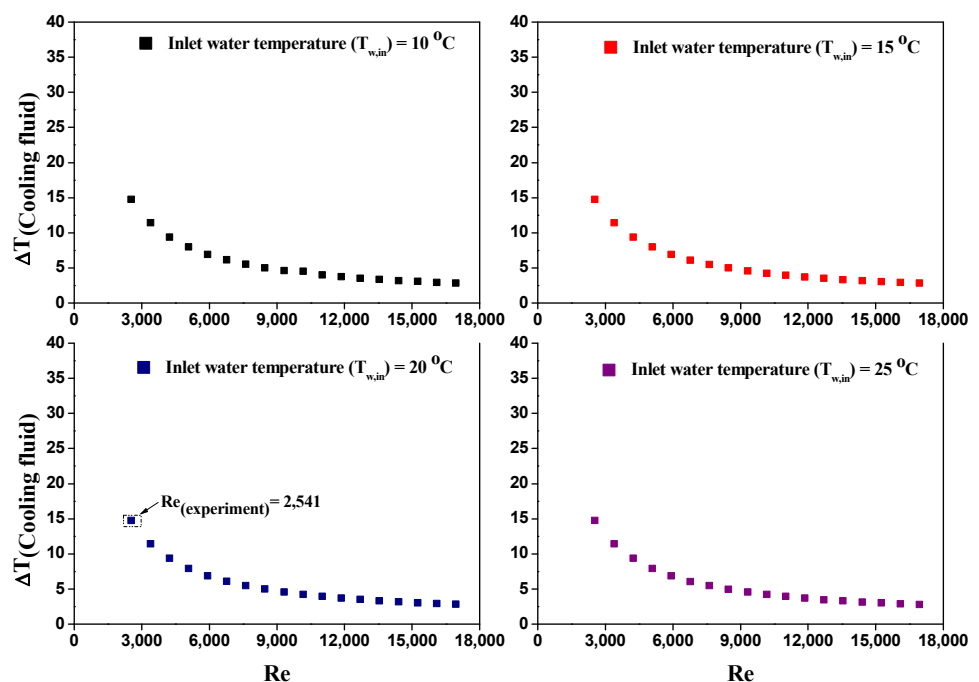


**Figure 11.** Variation in cold water temperature difference.

Figure 12 shows the variation in hot- and cold-side TEG temperature difference with varying flow rate at various inlet temperatures of cooling water. Initially, the rate of change in the hot- and cold-side TEG temperature difference increases with an increase in flow rate up to Re = 4235, with the rate of change in temperature difference flattening after Re = 4235. The effect of inlet water temperature on TEG heat transfer characteristics can be seen, with the highest heat transfer observed for the lowest inlet water temperature of 10 °C. This may be due to the fact that higher heat transfer takes place at lower temperatures.
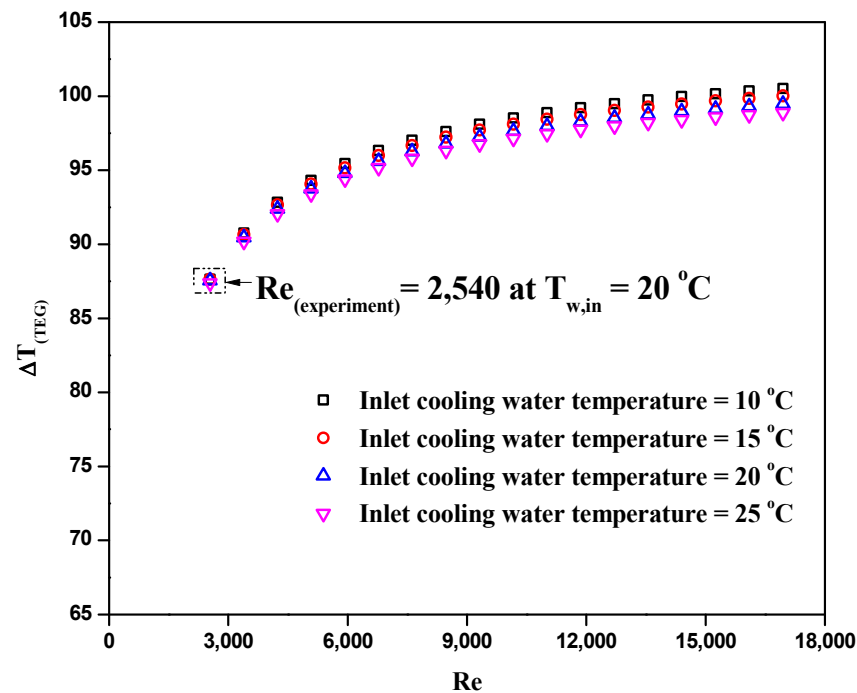
**Figure 12.** Variation in hot- and cold-side temperature difference.

The attempt has also been made to evaluate the auxiliary power consumption of the cooling system for the one module of set-1a, and it is found to be 0.046 W for the mass flow rate (0.03 kg/s) used in the experiment as evaluated by Jang et al. [16]. It is worth noticing that the power consumed by cooling system to cool one module is 1.3% of the power produced by one module at the operating voltage of the battery, and therefore, the net power produced by one module is found to be 3.484 W and the corresponding net efficiency is found to be 1.42% in the experimental study. Here, one can see that the net produced power is not much affected during experiments. However, a net produced power is found to be affected significantly with the increase in water flow rate (0.03−2.0 kg/s) during numerical investigation. The power consumed by the cooling system to cool one module is found to vary up to 6.3% for a water mass flow rate of 2.0 kg/s at 25 °C of inlet temperature of water. Therefore, the net power produced by the one module is considered during the numerical investigation. In view of this, efforts have been made to evaluate the highest net power output of one module of TEG set-1a (Figure 13) using the MPPT model. The maximum net power of the module increases with an increase in the cooling water flow rate and a decrease in the inlet temperature of the cooling water. Figure 14 depicts the variation in the maximum net efficiency of set-1a of the TEG system, corresponding to the maximum net power output following the MPPT model, while varying the cooling water flow rate and inlet temperature. It has been observed that the net efficiency of the TEG system increases with an increase in the cooling flow rate of water and with a decrease in the inlet water temperature. Higher heat transfer occurs at lower inlet water temperatures, and a higher cooling flow rate results in an increase in the thermal characteristics of the TEG system. This may be the reason for the increase in the maximum net power output and the increase in the corresponding net efficiency of the TEG module following the MPPT model.
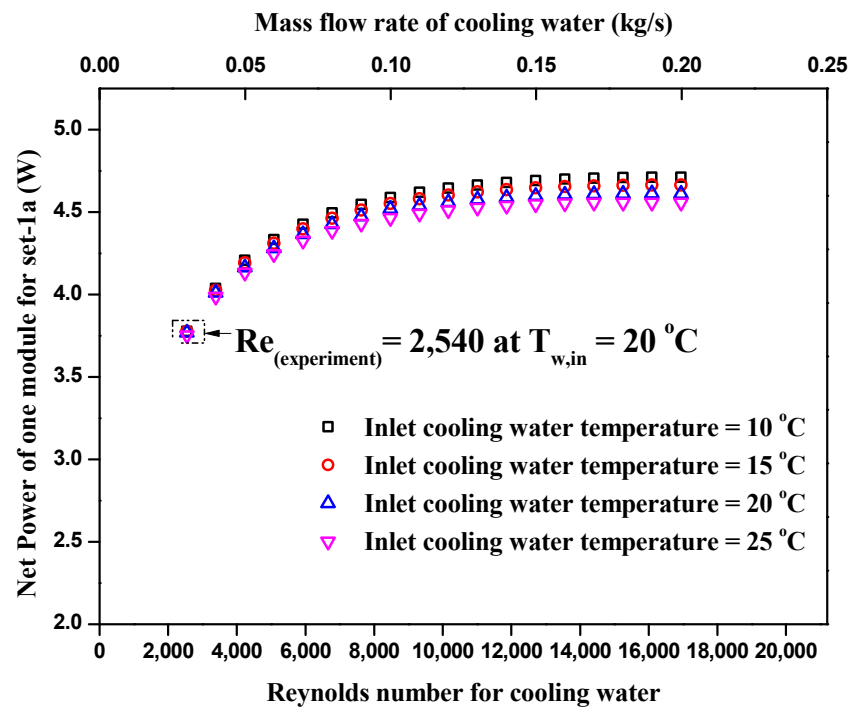
**Figure 13.** Variation in maximum net power output of one module of TEG set-1a.
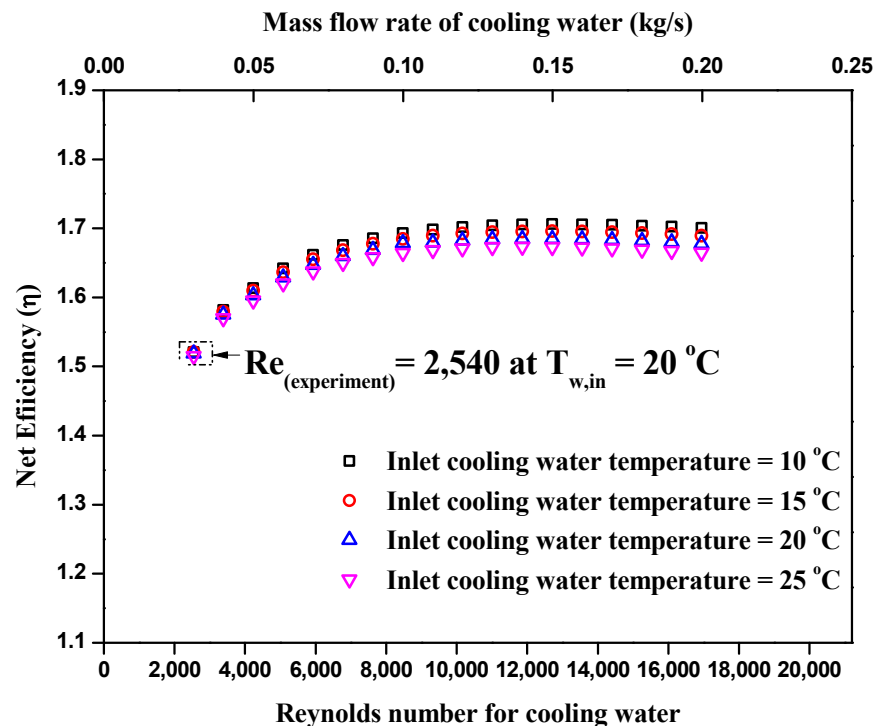


**Figure 14.** Variation in maximum net efficiency of TEG set-1a.

## 5. Conclusions

In the present study, experiments were performed to recover the waste heat during the cooling process of billet casting to improve the power density of a thermoelectric generator system using a d-type absorber plate. The waste heat was recovered to generate power using a bismuth telluride-based thermoelectric generator attached to four d-type absorber plates coupled with TEGs on three sides of each absorber plate set. In addition, one-dimensional numerical simulation was carried out utilizing commercially available

software FloMASTERTM to validate the experimental results for the steady-state heat transfer for one of the absorber plate sets (set-1a). Results were obtained for the hot- and cold-side TEG temperatures, and finally, the power output from the TEG system was evaluated. The simulation results showed good agreement with the experimental results. The average temperature for the hot side TEG was 207.5 °C in the experimental investigation, while it was 215.3 °C in the numerical simulation. The experimental and numerical results for the cold-side TEG temperature were 122.2 and 127.7 °C, respectively. The power density of the TEG was found to improve using a d-type absorber plate. The power density of the TEG system was 981 and 1027 W/m² in experimental and numerical investigations, respectively, while using the TEG system at an operating voltage of 58 V for the energy storage system. Using the MPPT model, the maximum power densities were found to be 1002 and 1061 W/m² through experimental and numerical analyses, respectively. Utilizing the MPPT model and considering auxiliary power consumption of coolant water, maximum net power density was found to be 967.7 W/m² and 1015 W/m² in experimental and numerical investigation, respectively. In addition, using a one-dimensional numerical simulation, the results obtained for varying the flow rate and inlet temperature of water at the cold side of the TEG indicated a higher performance of the TEG system at the lowest inlet temperature and highest flow rate of the coolant.

**Author Contributions:** S.Y. and J.L. performed the experimental and numerical analyses and drafted the manuscript. M.S.K. and Y.G.Y. discussed the results. S.C.K. organized the overall evaluation and reviewed the manuscript. All authors have read and agreed to the published version of the manuscript.

**Institutional Review Board Statement:** Not applicable.

**Informed Consent Statement:** Not applicable.

**Data Availability Statement:** Not applicable.

**Conflicts of Interest:** The authors declare no conflict of interest.

## Abbreviations

**Nomenclatures**

| | |
|---|---|
| $A$ | Area [m²] |
| $D$ | Diameter [m] |
| $DC$ | Direct current [a] |
| $H$ | Height [m] |
| $h$ | Heat transfer coefficient [W/m²-K] |
| $I$ | Current [a] |
| $K$ | Conductivity [W/m-K] |
| $L$ | Length [m] |
| $\dot{m}$ | Mass flow rate [kg/s] |
| $P$ | Power [W] |
| $Q$ | Heat flux [W/m²] |
| $R$ | Resistance [Ω] |
| $T$ | Temperature [°C] |
| $TEG$ | Thermoelectric generator [-] |
| $U$ | Overall heat transfer coefficient [W/m²-K] |
| $V$ | Voltage [V] |
| $W$ | Width [m] |

**Greek Symboles**

| | |
|---|---|
| $\alpha$ | Seebeck coefficient [$\mu$V/K] |
| $\varepsilon$ | Emissivity [-] |
| $\sigma$ | Stefan-Boltzmann constant [W/m$^2$-K$^4$] |
| $\eta$ | Efficiency [-] |

**Subscripts**

| | |
|---|---|
| *a* | Absorber plate (TEG side) |
| *ab* | Absorber plate (billet side) |
| *Avg* | Average |
| *b* | Billet |
| *c* | Cold |
| *cp* | Cooling plate |
| *c,t* | Cold-side TEG |
| *cw* | Cold water |
| *ex* | External |
| *exp* | Experimental |
| *h* | Hot |
| *h,t* | Hot-side TEG |
| *m* | Module |
| *max* | Maximum |
| *pn* | *p*- and *n*-type semiconductors |

## References

1. Jaziri, N.; Boughamoura, A.; Müller, J.; Mezghani, B.; Tounsi, F.; Ismail, M. A comprehensive review of Thermoelectric Generators: Technologies and common applications. *Energy Rep.* **2020**, *6*, 264–287. [CrossRef]
2. Daniel, C. Thermoelectric generators: A review of applications. *Energy Convers. Manag.* **2017**, *140*, 167–181.
3. Forman, C.; Muritala, I.K.; Pardemann, R.; Meyer, B. Estimating the global waste heat potential. *Renew. Sustain. Energy Rev.* **2016**, *57*, 1568–1579. [CrossRef]
4. Firth, A.; Zhang, B.; Yang, A. Quantification of global waste heat and its environmental effects. *Appl. Energy* **2019**, *235*, 1314–1334. [CrossRef]
5. Huang, F.; Zheng, J.; Baleynaud, J.M.; Lu, J. Heat recovery potentials and technologies in industrial zones. *J. Energy Inst.* **2017**, *90*, 951–961. [CrossRef]
6. Jouhara, H.; Khordehgah, N.; Almahmoud, S.; Delpech, B.; Chauhan, A.; Tassou, S.A. Waste heat recovery technologies and applications. *Therm. Sci. Eng. Prog.* **2018**, *6*, 268–289. [CrossRef]
7. Kaibe, H.; Makino, K.; Kajihara, T.; Fujimoto, S.; Hachiuma, H. Thermoelectric generating system attached to a carburizing furnace at Komatsu Ltd., Awazu Plant. *AIP Conf. Proc.* **2012**, *1449*, 524–527.
8. Aranguren, P.; Astrain, D.; Pérez, M.G. Computational and experimental study of a complete heat dissipation system using water as heat carrier placed on a thermoelectric generator. *Energy* **2014**, *74*, 346–358. [CrossRef]
9. Aranguren, P.; Astrain, D.; Rodriguez, A.; Martinez, A. Experimental investigation of the applicability of a thermoelectric generator to recover waste heat from a combustion chamber. *Appl. Energy* **2015**, *152*, 121–130. [CrossRef]
10. Kuroki, T.; Murai, R.; Makino, K.; Nagano, K.; Kajihara, T.; Kaibe, H.; Hachiuma, H.; Matsuno, H. Research and development for thermoelectric generation technology using waste heat from steelmaking process. *J. Electron. Mater.* **2015**, *44*, 2151–2156. [CrossRef]
11. Kuroki, T.; Kabeya, K.; Makino, K.; Kajihara, T.; Kaibe, H.; Hachiuma, H.; Matsuno, H.; Fujibayashi, A. Thermoelectric generation using waste heat in steel works. *J. Electron. Mater.* **2014**, *43*, 2405–2410. [CrossRef]
12. Kajihara, T.; Makino, K.; Lee, Y.H.; Kaibe, H.; Hachiuma, H. Study of thermoelectric generation unit for radiant waste heat. *Mater. Today Proc.* **2015**, *2*, 804–813. [CrossRef]
13. Ebling, D.G.; Krumm, A.; Pfeiffelmann, B.; Gottschald, J.; Bruchmann, J.; Benim, A.C.; Adam, M.; Labs, R.; Herbertz, R.R.; Stunz, A. Development of a system for thermoelectric heat recovery from stationary industrial processes. *J. Electron. Mater.* **2016**, *45*, 3433–3439. [CrossRef]
14. Yazawa, K.; Shakouri, A.; Hendricks, T.J. Thermoelectric heat recovery from glass melt processes. *Energy* **2017**, *118*, 1035–1043. [CrossRef]
15. Luo, Q.; Li, P.; Cai, L.; Zhou, P.; Tang, D.; Zhai, P.; Zhang, Q. A thermoelectric waste-heat-recovery system for Portland cement rotary kilns. *J. Electron. Mater.* **2015**, *44*, 1750–1762. [CrossRef]
16. Jang, J.Y.; Tsai, Y.C.; Wu, C.W. A study of 3-D numerical simulation and comparison with experimental results on turbulent flow of venting flue gas using thermoelectric generator modules and plate fin heat sink. *Energy* **2013**, *53*, 270–281. [CrossRef]
17. Børset, M.T.; Wilhelmsen, Ø.; Kjelstrup, S.; Burheim, O.S. Exploring the potential for waste heat recovery during metal casting with thermoelectric generators: On-site experiments and mathematical modelling. *Energy* **2017**, *118*, 865–875. [CrossRef]

18. Cao, Q.; Luan, W.; Wang, T. Performance enhancement of heat pipes assisted thermoelectric generator for automobile exhaust heat recovery. *Appl. Therm. Eng.* **2018**, *120*, 1472–1479. [CrossRef]

19. Remeli, M.F.; Date, A.; Orr, B.; Ding, L.C.; Singh, B.; Affandi, N.D.N.; Akbarzadeh, A. Experimental investigation of combined heat recovery and power generation using a heat pipe assisted thermoelectric generator system. *Energy Convers. Manag.* **2016**, *111*, 147–157. [CrossRef]

20. Kang, J.O.; Kim, S.C. Heat Transfer Characteristics of Heat Exchangers for Waste Heat Recovery from a Billet Casting Process. *Energies* **2019**, *12*, 2695. [CrossRef]